ACS OMEGA

http://pubs.acs.org/journal/acsodf

Article

Symmetric Growth of Dual-Packed Kernel: Exploration of the Evolution of $Au_{40}(SR)_{24}$ to $Au_{49}(SR)_{27}$ and $Au_{58}(SR)_{30}$ Clusters via the $2e^-$-Reduction Cluster Growth Mechanism

Lin Xiong and Yong Pei*

Cite This: *ACS Omega* 2021, 6, 18024−18032

Read Online

ACCESS | Metrics & More | Article Recommendations | Supporting Information

ABSTRACT: The symmetric and periodic growth of metal core and ligand shell has been found in a number of ligand-protected metal clusters. So far, the principle of symmetric growth has been widely used to understand and predict the cluster structure evolution. In this work, based on the experimentally resolved crystal structure of $Au_{40}(o\text{-MBT})_{24}$ and $Au_{49}(2,4\text{-DMBT})_{27}$ clusters and a newly proposed two-electron ($2e^-$) reduction cluster growth mechanism, the evolution pathway from the quasi-face-centered-cubic (fcc)-structured $Au_{40}(SR)_{24}$ cluster to the dual fcc- and nonfcc-packed $Au_{49}(SR)_{27}$ and $Au_{58}(SR)_{30}$ clusters was studied. The current research has clarified two important issues of cluster structure evolution. First, the formation of the dual-packed fcc and nonfcc kernel structure has been rationalized based on a $2e^-$reduction-based seed-mediated cluster growth pathway. Second, it is found that the symmetrical growth does not necessarily lead to the formation of stable cluster structures. It was found that the formation of dual-packed kernels in the $Au_{49}(SR)_{27}$ cluster is favorable because of the stability of the intermediate cluster structures and the relatively high thermodynamic stability of the cluster itself. However, although the structure of $Au_{58}(SR)_{30}$ cluster conforms to the principle of symmetric growth, the tension between the ligand shell and the gold atom of the metal nucleus increases significantly during the cluster size evolution, and the stability of the intermediate clusters is poor, so the formation of the $Au_{58}(SR)_{30}$ cluster is unfavorable. This study also shows that the $2e^-$-reduction cluster growth mechanism can be used to explore the structural evolution and stability of thiolate-protected gold clusters.

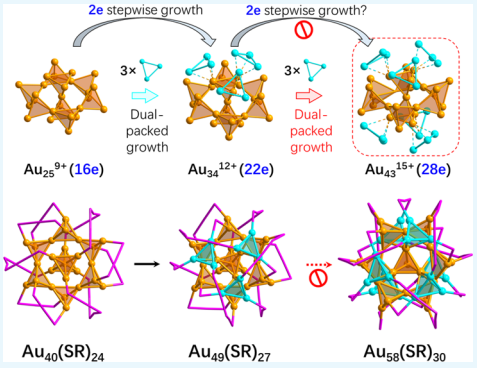

1. INTRODUCTION

Ligand-protected noble-metal clusters have become a research hotspot in the field of nanoscience because of their unique physicochemical properties.[1−6] In particular, because of the relatively excellent chemical stability of thiolate-protected gold nanoclusters (usually referred to as the $Au_n(SR)_m^q$ cluster, hereinafter denoted as RS-AuNCs), tremendous efforts have been devoted to the study of the structure and properties of such clusters.[3,5,7−17] Pioneered by the breakthrough of successful crystallization of the $Au_{102}(SR)_{44}$ cluster in 2007,[18] a large amount of RS-AuNCs has been experimentally crystallized, and precise atomic structures were characterized.[3] On this basis, researchers can further explore the evolution of cluster structures and the structure−property relationship in order to understand more clearly the role of clusters as a mesoscopic substance in the process of connecting micro and macromatter and to develop its potential applications.[3,8,19−21]

X-ray single crystal diffraction analyses showed that the RS-AuNCs consisted of a symmetrical gold core and outer staple motifs.[7] Until 2012, it was found that almost all the determined atomic structures of thiolate and the mixed phosphine/halide/thiolate-protected gold nanoclusters contained multiple-twinned gold core structures, and the icosahedron or its derivate served as the basic structural units of gold core.[22−27] As more unprecedented stable cluster sizes and cluster structures were determined, it was discovered that these clusters showed different configurations of core structures, such as icosahedron, dodecahedron, face-centered cubic (fcc), hexagonal closet packing (hcp), and body-centered cubic (bcc) configurations.[3,17]

These resolved cluster crystal structures revealed some inherent structural evolution patterns, among which a typical evolution pattern is symmetry or periodicity.[11,28] For example, the core structures of $Au_{21}(SR)_{15}$[11,29] and $Au_{23}(SR)_{16}^-$[30] clusters can be seen as one and two triangular Au_3, growing symmetrically on both sides of the Au_7 core of $Au_{20}(SR)_{16}$,[31] respectively. A similar case of symmetric growth occurs in the sequences of $Au_{28}(SR)_{20}$[32] → $Au_{29}(SR)_{19}$[33,34] → $Au_{30}(SR)_{18}$[35] and $Au_{44}(SR)_{28}$[36] → $Au_{68}(SR)_{36}$[37] → $Au_{92}(SR)_{44}$,[38] although

Received: April 3, 2021
Accepted: June 3, 2021
Published: July 7, 2021

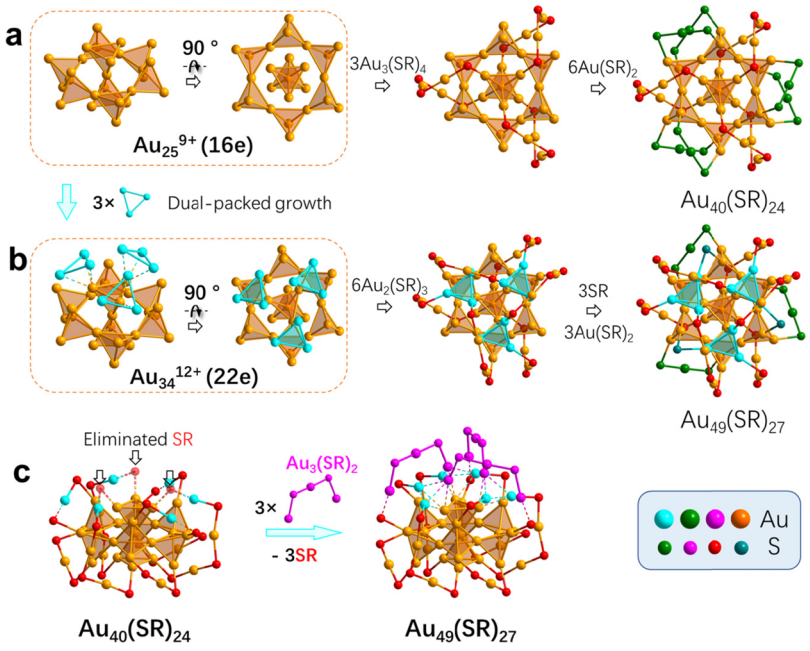

Figure 1. Comparative analysis of the gold core and the Au-SR ligand motifs of the $Au_{40}(SR)_{24}$ and $Au_{49}(SR)_{27}$ clusters. (a, b) Structural anatomy and (c) structural differences between $Au_{40}(SR)_{24}$ and $Au_{49}(SR)_{27}$.

the structure of $Au_{68}(SR)_{36}$ have not been experimentally confirmed. The gold quantum boxes, including the Au_{28}, Au_{36}, Au_{44}, and Au_{52} magic series, reported by Jin et al., can also be regarded as a result of growing Au_3 triangles symmetrically on both sides of the double Au_7 core, starting from $Au_{28}(TBBT)_{20}$.[36] Based on the experimentally determined cluster structures, a structure evolution map of the fcc-structured RS-AuNCs has been further proposed recently, which revealed the basic evolution pattern of RS-AuNC cluster containing an fcc core.[11]

Although the symmetric growth has been found in a number of ligand-protected gold clusters and the principle has been used to understand and predict the structural evolution of ligand-protected gold clusters, the following question is raised: is the symmetric growth an eternal law in the evolution of RS-AuNCs? Recently, the new progress in the experimental studies indicated that the kernel atoms of RS-AuNCs can be packed into a dual-packed kernel configuration.[39−41] Such a dual-packed kernel cluster exhibited a subnanoscale heterojunction structure. Through the density functional theory (DFT) calculations, an interesting finding was obtained: the highest occupied molecular orbitals (HOMOs) and the lowest unoccupied molecular orbitals (LUMOs) of dual-packed kernel Au_{49}(2,4-DMBT)$_{27}$ cluster are distributed in the fcc and nonfcc components of gold kernels, respectively.[40] Further experimental studies revealed that kernel packing greatly influences the electrochemical gap (EG), and the fcc structure exhibits a larger EG than the investigated nonfcc structure. Because the EG is correlated to some fundamental physicochemical properties of the materials, such dual-packed kernel metal clusters were expected to possess novel electronic and optical properties compared with the regular icosahedral or fcc gold clusters. Another prototype of dual-packed kernel clusters was found in a low-temperature isomer of the $Au_{38}(SC_2H_4Ph)_{24}$ cluster.[41] In the isomeric $Au_{38}(SC_2H_4Ph)_{24}$ cluster, the metal core was composed of an icosahedral Au_{13} and a group of fcc-structured Au atoms. The newly discovered dual-packed kernel clusters implied a new evolution pathway of the RS-AuNCs, which raised interesting questions with regard to the cluster structure evolution and growth mechanism. The first question is as follows: is there a new cluster sequence with the core structure that adopts a hybrid dual-packed fcc and nonfcc configuration? The second question is as follows: What is the formation mechanism of the dual-packed kernel structures? The last but not least, is the principle of symmetric growth maintained in the evolution of clusters?

In this study, based on the crystal structure of the Au_{40}(*o*-MBT)$_{24}$[42] and Au_{49}(DMBT)$_{27}$[40] clusters, we explored the evolution pathway from the fcc-structured $Au_{40}(SR)_{24}$ to the dual-packed fcc and nonfcc clusters $Au_{49}(SR)_{27}$ and $Au_{58}(SR)_{30}$. The coordinate files of the clusters involved in the evolution path are presented in the Supporting Information. Very recently, we noted that Xu et al. predicted the atomic structure of $Au_{58}(SR)_{30}$ based on the symmetric growth of the nonfcc part of the $Au_{49}(SR)_{27}$ cluster.[43] Their predicted cluster structure is consistent with that of the Au_{58}-iso2 in this study. Different from the previous report, this work reported a very comprehensive study on the formation mechanism of the nonfcc kernel structure on the $Au_{49}(SR)_{27}$ and $Au_{58}(SR)_{30}$ clusters based on a newly proposed $2e^-$reduction-assisted seed-mediated cluster evolution mechanism.[44] An evolution pathway from the $Au_{40}(SR)_{24}$ to the $Au_{49}(SR)_{27}$ and then to the $Au_{58}(SR)_{30}$ was mapped out first based on the $2e^-$-reduction cluster growth mechanism, which explained the formation of the nonfcc kernel structure on the $Au_{49}(SR)_{27}$ and the $Au_{58}(SR)_{30}$ clusters. More importantly, the mapped evolution pathway enabled us to assess the stability of the intermediate and the product clusters with the dual-packed kernel. In the present study, energy evaluation by the DFT calculations showed that the formation of dual-packed kernel intermediate clusters $Au_{43}(SR)_{25}$, $Au_{46}(SR)_{26}$, and $Au_{49}(SR)_{27}$ is energetically favorable. However, the latter cluster evolution pathway from $Au_{49}(SR)_{27}$ to $Au_{58}(SR)_{30}$ was unfavorable in terms of both poor thermodynamic stability of intermediate

https://doi.org/10.1021/acsomega.1c01791
ACS Omega 2021, 6, 18024−18032

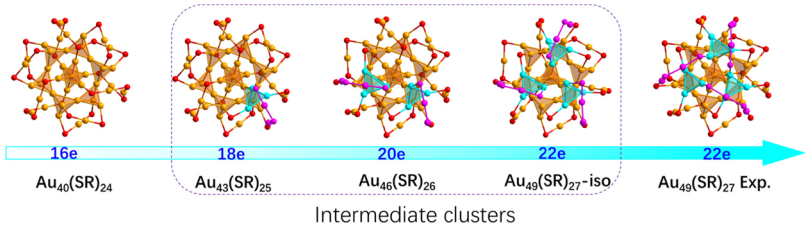

Figure 2. Constructed structures of intermediate clusters $Au_{43}(SR)_{25}$, $Au_{46}(SR)_{26}$, and $Au_{49}(SR)_{27}$-iso. Color labels: Turquoise, newly added Au atoms in the gold core during size evolution; Light orange, Au; pink, Au and sulfur in foreign fragments; red, sulfur. The R groups are omitted for clarity.

clusters (i.e., $Au_{52}(SR)_{28}$ and $Au_{55}(SR)_{29}$) in the size-growth process and the low stability of the dual-packed structure of $Au_{58}(SR)_{30}$. Therefore, although the $Au_{58}(SR)_{30}$ conformed to the principle of the symmetric growth of the cluster structure, its low thermodynamic stability may not be conducive to its formation. This study also suggested that in order to study the evolution of clusters, it is necessary to comprehensively study the structural stability of clusters and the thermodynamics of the formation process. The $2e^-$ reduction-assisted cluster size growth mechanism is a good scenario to explore the structure evolution, stability, and formation process of RS-AuNCs.

2. COMPUTATIONAL METHOD AND DETAILS

In this work, the cluster structural optimizations were performed by DFT, with the R groups simplified with CH_3. The Perdew–Burke–Ernzerhof (PBE) functional[45] and the d-polarization basis set (DND) were used for the elements C, H, and S. The DFT semicore pseudopotential (DSPP) approximation with some degree of relativistic correction into the core was used for Au implemented in the Dmol^3 package.[46,47] The dispersion effect was considered in the structural optimization and calculations of the transition state (TS) using the Tkatchenko and Scheffler method.[48] In addition, in order to get closer to the experimental facts, the conductor-like screening model (COSMO) solvent model[49] was adopted to reflect the solvent effect with water as the solvent. The time-dependent DFT (TD-DFT), as implemented in the Amsterdam density functional (ADF) software package,[50] was utilized for calculating the ultraviolet–visible (UV–vis) spectra of the as-predicted cluster sequence. The triple-zeta polarized (TZP) basis set with the inclusion of the scalar relativistic effect via a zeroth-order regular approximation (ZORA) implemented in the ADF package was adopted. The TD-DFT calculations evaluated the lowest 500 singlet-to-singlet excitation energies. The structures of the clusters involved in the spectral calculations in this work are relatively large. Considering that the cluster structures do not change significantly after the ligands are replaced by the H atoms, we therefore use H atoms as substituents to simplify the ligands to save computational costs. Such spectral accuracy is sufficient for the qualitative analysis of the optical absorption characteristics of the gold clusters.

3. RESULTS AND DISCUSSION

3.1. Evolution Pathway of Cluster Structures from $16e^-$ $Au_{40}(SR)_{24}$ to $22e^-$ $Au_{49}(SR)_{27}$.

Figure 1a,b displays the structure anatomy of the $Au_{40}(SR)_{24}$ and $Au_{49}(SR)_{27}$ clusters. According to the "divide-and-protected" scheme,[51,52] the two clusters can be formulated as $Au_{25}[Au(SR)_2]_6[Au_3(SR)_4]_3$ and $Au_{34}(SR)_3[Au(SR)_2]_3[Au_2(SR)_3]_6$, respectively. Considering that each bridge SR group or $[Au_x(SR)_y]$ motif can bind one Au-6s electron, the total number of free valence electrons of the $Au_{40}(SR)_{24}$ and $Au_{49}(SR)_{27}$ clusters was 16 and 22, respectively, and the Au core in the two clusters can be viewed as Au_{25}^{9+} and Au_{34}^{12+}, respectively. For both clusters, they showed a good relationship between the total number of free valence electrons and the polyhedron building blocks in the metal core. Our recent studies suggested that the tetrahedron-Au_4 and the triangle-Au_3 unit in the RS-AuNCs can be viewed as the basic $2e^-$ building block, that is, Au_4^{2+} or Au_3^+.[11] Based on this viewpoint, the $16e^-$ and $22e^-$ of $Au_{40}(SR)_{24}$ and $Au_{49}(SR)_{27}$ clusters correspond to their unique metal core stacking configurations. As shown in Figure 1a,b, the gold core in $Au_{40}(SR)_{24}$ was made of eight vertex-shared Au_4 tetrahedra. Each Au_4 tetrahedron can be considered as a $2e^-$ unit (Au_4^{2+}). As for the $Au_{49}(SR)_{27}$ cluster, the $22e^-$ originates from 11 Au_4^{2+} units.

In view of the structure of the gold core of Au_{40} and Au_{49} clusters, the gold core in Au_{40} has a fcc-geometry made of a central Au_7 bi-tetrahedron and a Kekulé ringlike conjugated Au_4 tetrahedron ring,[42] while the gold core in the Au_{49} cluster can be regarded as adding three new Au_3 triangular units to the gold core of the Au_{40} cluster.[40] Based on the structures of the gold cores in the Au_{40} and Au_{49} clusters, a new cluster size growth mechanism may be implied. Quite evidently, there are some intermediate clusters in the size evolution from Au_{40} to Au_{49}. Exploring the geometries and relative stabilities of these intermediate clusters will enable us to gain a deeper understanding of the evolutionary mechanism of the RS-AuNCs.

As shown in Figure 1b, the Au core of the $Au_{49}(SR)_{27}$ cluster can be evolved from the Au core of the $Au_{40}(SR)_{24}$ cluster by "growing" three triangular Au_3 units on the vertex of three symmetric Au_4 tetrahedra. At the same time, three trimeric staples on one side of the Au_{40} cluster lose three SR groups (the transparent red ball in Figure 1c), and the trimeric staple and its adjacent monomer staple each has an Au atom (turquoise balls) that contributes to the formation of a newly added Au_3 unit. Because of the growth of three new triangle Au_3 units and the rearrangement of the ligand motifs, the gold core of the $Au_{49}(SR)_{27}$ cluster forms a hybrid fcc and nonfcc dual-packed configuration.

Based on the analysis on the structure and valence electron number of the $Au_{40}(SR)_{24}$ and $Au_{49}(SR)_{27}$ clusters, a stepwise $2e^-$ evolution pathway is suggested. It proposes that the $Au_{49}(SR)_{27}$ cluster can be evolved from the $Au_{40}(SR)_{24}$ cluster by the sequential growth of Au_4 tetrahedra and ligand motifs, that is, $Au_{40}(SR)_{24}$ ($16e^-$) + $Au_3(SR)_1$ → $Au_{43}(SR)_{25}$ ($18e^-$) + $Au_3(SR)_1$ → $Au_{46}(SR)_{26}$ ($20e^-$) + $Au_3(SR)_1$ → $Au_{49}(SR)_{27}$ ($22e^-$). In the proposed cluster evolution pathway, $Au_{43}(SR)_{25}$ and $Au_{46}(SR)_{26}$ are two intermediate clusters, and their

https://doi.org/10.1021/acsomega.1c01791
ACS Omega 2021, 6, 18024–18032

Scheme 1. Explanation of the Proposed Carboxylation−Decarboxylation Reaction Mechanism Based on CO Reduction. Turquoise, Au Atoms in Staple Motifs; Pale Blue, Au Atoms in Gold Core; Yellow, Sulfur; Red, Oxygen; Gray, Carbon; White, Hydrogen. R Groups Are Omitted for Clarity

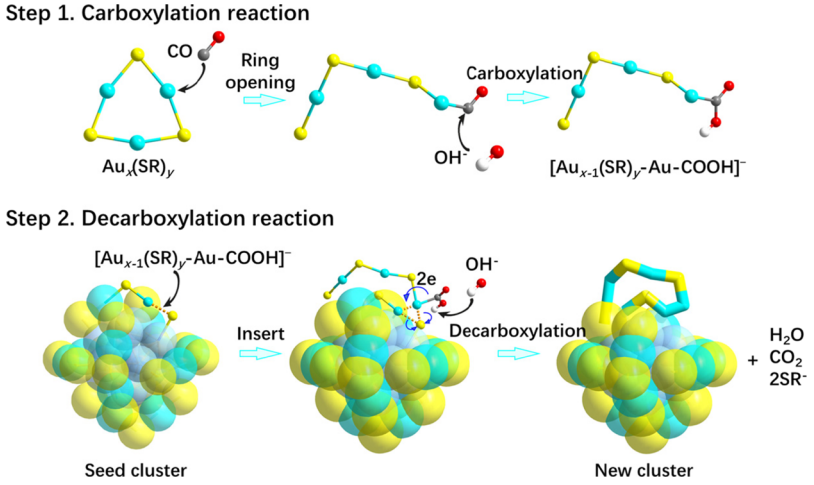

structures can be constructed based on $Au_{40}(SR)_{24}$ by adding one or two $Au_3(SR)_1$ units, as shown in Figure 2.

The mapped structural evolution pathway displayed in Figure 2 implies a seed-mediated cluster growth mechanism. That is, $Au_{40}(SR)_{24}$ can be viewed as a seed cluster. Upon reacting with the thiolate−gold complexes (e.g., three $[Au_3(SR)_3]$) under the reductive environment, it may gradually grow into a larger-size $Au_{49}(SR)_{27}$ cluster through three $2e^-$-incrementation steps. The seed-mediated cluster growth process can be therefore formulated as eqs 123, where the $2e^-$ in each cluster size growth step comes from the reduction reagent such as $NaBH_4$ or CO.

$$Au_{40}(SR)_{24} + [Au_3(SR)_3] + 2e^- \rightarrow Au_{43}(SR)_{25} + 2SR^- \quad (1)$$

$$Au_{43}(SR)_{25} + [Au_3(SR)_3] + 2e^- \rightarrow Au_{46}(SR)_{26} + 2SR^- \quad (2)$$

$$Au_{46}(SR)_{26} + [Au_3(SR)_3] + 2e^- \rightarrow Au_{49}(SR)_{27} + 2SR^- \quad (3)$$

The theoretical speculated seed-mediated cluster growth process is supported by the recent experimental observation of the seed-mediated growth of RS-AuNCs. Xie et al. found that in the reduction environment, the magic stable $Au_{25}(SR)_{18}^-$ ($8e^-$) cluster can irreversibly grow into larger-size $Au_{38}(SR)_{24}$ ($14e^-$) and $Au_{44}(SR)_{26}$ ($18e^-$) clusters, and the size growth of clusters demonstrated clear stepwise $2e^-$ increamentations.[53] Based on the above discussion, we have manually constructed the structure of intermediate clusters $Au_{43}(SR)_{25}$, $Au_{46}(SR)_{26}$, and $Au_{49}(SR)_{27}$, and the structures of these intermediate clusters are displayed in Figure 2. Note that following the proposed $2e^-$-evolution pathway, the resulted $Au_{49}(SR)_{27}$ cluster has slightly different Au-S skeleton structure compared with the experimentally resolved structure of Au_{49}(2,4-DMBT)$_{27}$.[40] The theoretically constructed isomer structure was then referred to as $Au_{49}(SR)_{27}$-iso in this work. Herein, we focused on the geometric structure and the relative stabilities of the intermediate $Au_{43}(SR)_{25}$, $Au_{46}(SR)_{26}$, and $Au_{49}(SR)_{27}$-iso clusters. Very recently, Wu et al. reported the synthesis and crystal structure of the $Au_{43}(CHT)_{25}$ cluster (CHTH = cyclohexanethiol).[54] In contrast to the $Au_{43}(SR)_{25}$ cluster found in this work, the $Au_{43}(CHT)_{25}$ cluster reported in their work contained a quasi-fcc gold kernel. DFT calculations were performed to investigate the relative stabilities of two isomeric structures of $Au_{43}(SR)_{25}$ clusters. The results showed that the experimentally resolved structure was slightly stable than the theoretically proposed Au_{43} cluster by 0.29 eV (SR = SCH_3), which indicates that the newly constructed Au_{43} cluster structure model is energetically stable. On the other hand, we also compared the relative stability of $Au_{49}(SR)_{27}$-iso and the experimentally resolved structure of Au_{49}(2,4-DMBT)$_{27}$. It was found that the $Au_{49}(SR)_{27}$-iso in the evolution pathway is a higher-energy isomer compared with the experimental crystal structure, which is less stable by 0.47 eV (SR = SCH_3).

3.2. Seed-Mediated Cluster Size Growth Mechanism from $Au_{40}(SR)_{24}$ to $Au_{49}(SR)_{27}$. Because the Au_{40} and Au_{49} clusters demonstrated a clear structural evolution pattern in both the Au core and ligand motifs, an intriguing question is raised: can we find an evolutionary mechanism from Au_{40} to Au_{49} clusters? Recent studies of real-time monitoring of the bottom-up growth and the seed-mediated growth of water-soluble RS-AuNCs by UV−vis absorption and electrospray ionization mass spectrometry (ESI-MS) have revealed several valuable details of the formation and seed-mediated size-evolution mechanism of RS-AuNCs at the molecular- or even atomic level.[53,55] Among them, the seed-mediated growth of $Au_{44}(MBA)_{26}$ from $Au_{25}(MBA)_{18}$ in the mild CO-reduction system reported by Yao et al. clarified several fundamental puzzles of the NC field at the molecular level, especially the uncovering of an interesting gold cluster growth principle—the $2e^-$ hopping pathway.[53]

In the present study, the suggested stepwise $2e^-$-incrementation size-evolution pathway from Au_{40} to Au_{49} clusters agreed very well with the growth principle of water-soluble RS-AuNCs. Inspired by these experimental facts and combined with the $2e^-$-incrementation pathway displayed in Figure 2, here, we proposed a new mechanism to address the evolution process from the $Au_{40}(SR)_{24}$ cluster to the $Au_{49}(SR)_{27}$ cluster using CO as a model reduction agent. As mentioned in the reaction eqs 123, the size-evolution from the $Au_{40}(SR)_{24}$ cluster to $Au_{49}(SR)_{27}$ cluster can be divided into three $2e^-$-incrementation size-growth steps. In each cluster size-growth step, $2e^-$ reduction is required to achieve the growth of a new tetrahedron Au_4 unit in the core and the new

https://doi.org/10.1021/acsomega.1c01791
ACS Omega 2021, 6, 18024−18032

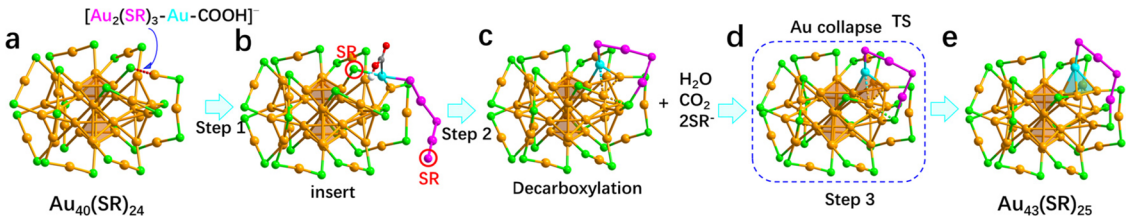

Figure 3. Illustration of the size evolution from $Au_{40}(SR)_{24}$ to $Au_{43}(SR)_{25}$ based on the carboxylation−decarboxylation mechanism using CO as the model reduction agent. (a) Framework of $Au_{40}(SR)_{24}$. (b) Carboxylated $Au_3(SR)_3$ fragment is inserted between an Au−S bond in the ligand of Au_{40}. (c) Process of decarboxylation. In this process, two SR groups (marked by red circles) are eliminated, which come from the Au_{40} and $Au_3(SR)_3$ fragments, respectively. (d) TS structure in the process of evolution from $Au_{40}(SR)_{24}$ to $Au_{43}(SR)_{25}$ (This process involves the collapse of motif Au). (e) Skeleton structure of $Au_{43}(SR)_{25}$. Light orange/pink/turquoise, Au atoms; bright green/pink, sulfur. R groups are omitted for clarity.

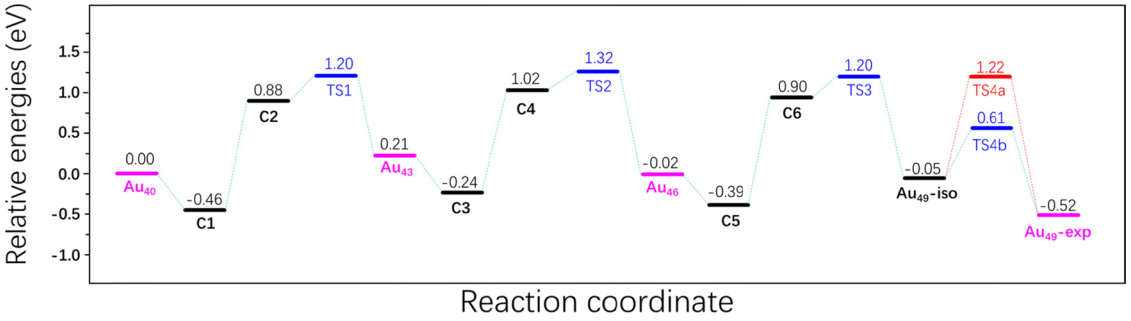

Figure 4. Energy curve of the dual-packed cluster sequence from $Au_{40}(SR)_{24}$ to $Au_{49}(SR)_{27}$-exp based on the carboxylation and decarboxylation mechanism. C1, C3, and C5 are cluster species formed by $Au_{40}(SR)_{24}$, $Au_{43}(SR)_{25}$, and $Au_{46}(SR)_{26}$ combined with one $[Au_3(SR)_3COOH]^-$ fragment, respectively. C2, C4, and C6 are the products of decarboxylation of $[Au_{40}(SR)_{24}\text{-}Au_3(SR)_3COOH]^-$, $[Au_{43}(SR)_{25}\text{-}Au_3(SR)_3COOH]^-$, and $[Au_{46}(SR)_{26}\text{-}Au_3(SR)_3COOH]^-$, respectively. TS1, TS2, and TS3 represent the transition states of motif Au collapse and nucleation. TS4a and TS4b indicate two different ways of isomerization between the Au_{49} isomers: the former is the rearrangement of the staples, and the latter is the rotation of the core.

ligand motifs. Here, using CO as a model reduction agent, Scheme 1 illustrates the basic idea of the newly proposed CO reduction-assisted $2e^-$ reduction-assisted gold cluster growth mechanism.[44]

In the first reaction step, an Au(I)−thiolate complex such as a $[Au_3(SR)_3]$ reacts with CO to form a $[Au_3(SR)_3\text{-}CO]$ species, which can further react with OH^- via a Hieber base reaction to generate a $[Au_3(SR)_3\text{-}COOH]^-$ species in the alkaline environment. This activation mechanism is essentially the same as that previously proposed by Xie et al.[53] However, different from Xie's proposal, we, herein, suggested a new intermolecular association mechanism to account for the gold-core formation and $2e^-$-hopping process. As illustrated in Scheme 1, if the $Au_{40}(SR)_{24}$ cluster is considered as a seed cluster, we propose that the $[Au_3(SR)_3\text{-}COOH]^-$ species may attach onto the surface of $Au_{40}(SR)_{24}$ by the insertion of the terminal Au-$COOH^-$ group between an Au−S bond on the surface of the seed cluster. This intermolecular association leads to the formation of a new anionic complex formulated $[Au_{40}(SR)_{24}][Au_3(SR)_3\text{-}COOH]^-$.

After the formation of the anionic complex, the $COOH^-$ group subjects a decarboxylation reaction with the OH^- in the solution. The decarboxylation reaction results in $2e^-$ injection, and the remaining $[Au_{40}(SR)_{24}][Au_3(SR)_3]$ complex has a −2 valence state. The $[Au_{40}(SR)_{24}][Au_3(SR)_3]^{2-}$ complex may further relax into the neutral state by the removal of two SR^- groups (Figure 3c). During this SR^- removal process, the terminal Au atom of the newly added $[Au_3(SR)_1]^-$ fragment bonded with a S atom. The resulted intermediate was formulated as $Au_{43}(SR)_{25}$. Then, the metastable $Au_{43}(SR)_{25}$ transforms into the more stable structure by collapsing a motif Au atom into the metal core, which bonded two metal-core gold atoms to form a new tetrahedron Au_4 unit, as shown in Figure 3d. The energy barrier of this Au atom migration process was only 0.32 eV. The whole process is described in Figure 3.

The cluster size growth process from $Au_{40}(SR)_{24}$ to $Au_{43}(SR)_{25}$ can be summarized as given in eq 4, where the $2e^-$ reduction and the growth of a new tetrahedron Au_4 unit and a new piece of the $[Au_3(SR)_4]$ motif fragment are achieved using carboxylation and decarboxylation processes. Once the $Au_{43}(SR)_{25}$ is formed, it can further grow into larger-size $Au_{46}(SR)_{26}$ and $Au_{49}(SR)_{27}$-iso clusters using two additional $2e^-$-reduction processes. Using CO as the reduction agent, the two cluster size growth reactions can be formulated as eqs 5 and 6, respectively. Figure S1 displays the details of these two clusters size growth steps. The energy profiles, as shown in Figure 4, indicate that the two cluster size growth processes are both energetically favorable.

$$Au_{40}(SR)_{24} + [Au_3(SR)_3] + CO + 2OH^- \rightarrow Au_{43}(SR)_{25} + H_2O + CO_2 + 2SR^- \quad (4)$$

$$Au_{43}(SR)_{25} + [Au_3(SR)_3] + CO + 2OH^- \rightarrow Au_{46}(SR)_{26} + H_2O + CO_2 + 2SR^- \quad (5)$$

$$Au_{46}(SR)_{26} + [Au_3(SR)_3] + CO + 2OH^- \rightarrow Au_{49}(SR)_{27} + H_2O + CO_2 + 2SR^- \quad (6)$$

An isomerization process is required to form the experimentally resolved $Au_{49}(SR)_{27}$ cluster from $Au_{49}(SR)_{27}$-

https://doi.org/10.1021/acsomega.1c01791
ACS Omega 2021, 6, 18024−18032

iso. Considering that the difference between the two clusters is mainly due to the arrangement of three ligand motifs on the surface (Figure 5a), we considered two isomerization pathways. As shown in Figure 5b, the first one, perhaps the most intuitive, is performed by the rearrangement of dimer motifs, which required breaking three Au−S bonds. DFT calculations show that the TS energy barrier of such a ligand-rearrangement process is 1.27 eV (TS4a in Figure 4). However, considering that the average distance between the three Au atoms (Au_1, Au_2, and Au_3 in Figure 5a) in the kernel of Au_{49}-iso (2.941 Å) is close to the Au−Au bond length in the core tetrahedral units, we assumed that the rotation of these three core Au atoms drives the outer ligand for distortion to occur, leading to isomerization of the structure (Figure 5c). The energy barrier of the TS generated in such an isomerization manner is 0.66 eV (TS4b in Figure 4). According to the Eyring equation,[56] it is estimated that such isomerization barriers can be crossed at room temperature. It is worth mentioning that Häkkinen et al. pointed out in their work that the chiral inversion of Au_{38} clusters does not need the break of the Au−S bonds (2.5 eV), but only the collective rotation (1−1.5 eV) of the core Au atoms can achieve the chiral inversion.[15] Therefore, we believe that the isomerization between the two Au_{49} is likely to be caused by the rotation of the Au_3 unit.

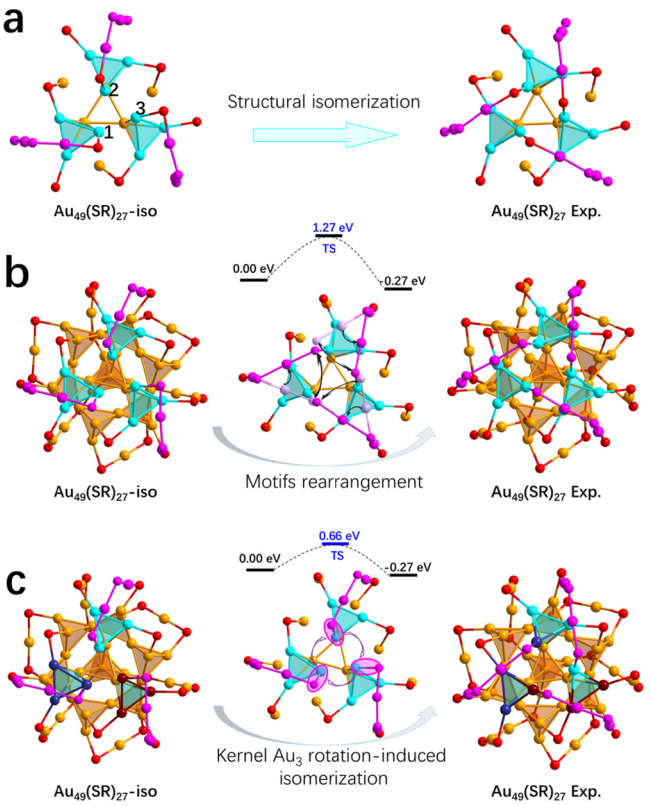

Figure 5. Structural differences and isomerization mechanism of two Au_{49} isomers. (a) Surface ligands of the two Au_{49} are arranged differently. (b) and (c) Two possible isomerization mechanism of two Au_{49} isomers. Light orange/turquoise/pink/dark red/plum/indigo, Au atoms; red/pink, sulfur. R groups are omitted for clarity.

The relative stabilities of $Au_{43}(SR)_{25}$, $Au_{46}(SR)_{26}$, and $Au_{49}(SR)_{27}$-exp were further examined by cluster transformation reaction eqs 789, respectively. The reactant clusters in these equations were adopted from the crystal structures or theoretical models.[36,37,57,58] The formation energy of the clusters is defined as E(products) − E(reactants), where E is the electronic energy. Using SCH_3 as the model SR group, the formation energies of $Au_{43}(SR)_{25}$, $Au_{46}(SR)_{26}$, and $Au_{49}(SR)_{27}$-exp are computed to be 0.42, 0.17, and 0.02 eV, respectively.

$$1/2[Au_{68}(SR)_{36} + Au_{18}(SR)_{14}] \rightarrow Au_{43}(SR)_{25} \quad (7)$$

$$1/2[Au_{68}(SR)_{36} + Au_{24}(SR)_{16}] \rightarrow Au_{46}(SR)_{26} \quad (8)$$

$$1/2[Au_{68}(SR)_{36} + Au_{30}(SR)_{18}] \rightarrow Au_{49}(SR)_{27} - exp \quad (9)$$

The favorable chemical and thermodynamic stabilities of the intermediate clusters were further demonstrated by DFT calculations. First, The HOMO−LUMO (H−L) gaps of clusters in this sequence are presented in Table S1. The value of H−L gaps gradually decreases from Au_{40} to Au_{49}-exp and then increases. Note that the H−L gap of Au_{49}-iso is relatively small, which can be attributed to its ligand motif arrangements. By isomerizing the ligand motifs, the Au_{49}-exp cluster not only demonstrates higher thermodynamic stability but also larger H−L gaps. Such a tendency confirms that the Au_{49}-iso tends to isomerize into the Au_{49}-exp. Second, as shown in Table S1, there is no imaginary frequency in the calculations of the frequencies of these clusters, indicating that all clusters are thermodynamically stable. The Cartesian coordinates of the as-predicted optimal structures of these clusters ($Au_{43}(SR)_{25}$, $Au_{46}(SR)_{26}$, and $Au_{49}(SR)_{27}$-iso) are shown in the Supporting Information. The UV−vis spectra of the as-predicted dual-packed clusters were also calculated, as shown in Figure S2.

3.3. Symmetric Growth of Dual-Packed Kernels from the $Au_{49}(SR)_{27}$ to $Au_{58}(SR)_{30}$ Cluster. A prominent feature of the structural evolution of the RS-AuNCs is that the clusters exhibited symmetric growth of the polyhedron core and ligand motifs. For instance, the one-dimensional (1D) symmetrical growth of double-helix tetrahedron Au_4 units was clearly identified according to the crystal structure of $Au_{28}(TBBT)_{20}$, $Au_{36}(TBBT)_{24}$, $Au_{44}(TBBT)_{28}$, and $Au_{52}(TBBT)_{32}$.[36] In addition, the centrosymmetric growth of triangular Au_3 units and ligand motifs from $Au_{28}(SR)_{20}$ to $Au_{30}(SR)_{18}$ clusters,[33] as well as the two-dimensional (2D) crystal face growth from $Au_{44}(SR)_{28}$ to $Au_{92}(SR)_{44}$ clusters[37] were also discovered.

In view of the nearly D_3 symmetry of the Au_{40} cluster, it is natural to consider whether or not the cluster size growth may happen on both sides of the cluster, which will lead to the formation of a larger-size cluster formulated $Au_{58}(SR)_{30}$, with symmetrical distribution of six newly added triangular Au_3 units. This new cluster size evolution process can be formulated as $Au_{49}(SR)_{27} + Au_1(SR)_3 \rightarrow Au_{52}(SR)_{28} + Au_1(SR)_3 \rightarrow Au_{55}(SR)_{29} + Au_1(SR)_3 \rightarrow Au_{58}(SR)_{30}$. During this process, three triangular Au_3 units are further formed on the $Au_{49}(SR)_{27}$. Based on this assumed evolution pathway, four new clusters, $Au_{52}(SR)_{28}$, $Au_{55}(SR)_{29}$, $Au_{58}(SR)_{30}$-iso1, and $Au_{58}(SR)_{30}$-iso2, are perspective. Note that the $Au_{58}(SR)_{30}$ (marked as Au_{58}-iso1) obtained through this growth mechanism may transform into the Au_{58}-iso2 via structural isomerization. The latter cluster was also predicted by Xu et al.[43] based on a similar symmetric evolution of the cluster structure. Herein, our DFT calculations showed that the Au_{58}-iso2 was 0.78 eV more stable than the Au_{58}-iso1, and the energy barrier of isomerization was determined to be 1.17 eV (Figure S3).

https://doi.org/10.1021/acsomega.1c01791
ACS Omega 2021, 6, 18024−18032

However, it is found that the optimized core structure of the product Au_{58}-iso2 cluster is significantly different from those of Au_{40} and Au_{49}-exp. As shown in Figure 6, the two conjugated

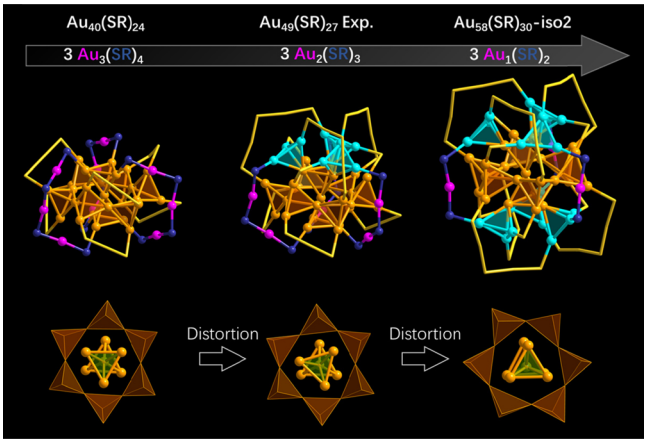

Figure 6. Comparison of the ligand layer structure and core structures of Au_{40}, Au_{49}-exp, and Au_{58}-iso2 clusters. R groups are omitted for clarify.

tetrahedron Au_4 units at the center of the Au_{58}-iso2 core adopt a consistent orientation. In terms of the overall cluster structure, three trimeric staples are gradually shortened to monomer staples in the process of Au_{40} to Au_{49} and then to Au_{58}. Correspondingly, the tension of the staples gradually increases. As a result, the core structure is distorted to a great extent. For instance, the two tetrahedron Au_4 units in the core with lower staple tension adopt a misalignment arrangement of about 60° in the Au_{40} cluster. After the growth of three new triangular Au_3 units and ligand motifs on one side, in the Au_{49}-exp, the relatively large tension caused by the shortening of the staples induces a slight twist in the two Au_4 units. Finally, to the Au_{58}-iso2, the orientations of these two Au_3 units overlaps, as shown in Figure 6.

The gradual structural distortion of gold cores from the Au_{49} to Au_{58} cluster displayed in Figure 6 prompts us to examine the stability of the cluster structures. It should be pointed out that it is difficult to quantitatively evaluate the intrinsic tension in the Au_{58}-iso2. Here, the relative stabilities of intermediate Au_{52}, Au_{55}, Au_{58}-iso2 clusters were evaluated by the reaction eqs 101112. It is found that unlike the favorable formation energy (0.17−0.49 eV) of Au_{43}, Au_{46}, and Au_{49}-iso clusters in the size-growth pathway from the $Au_{40}(SR)_{24}$ to $Au_{47}(SR)_{29}$ cluster, the formation energies of intermediate clusters such as Au_{52}, Au_{55}, and Au_{58}-iso2 in this new size-evolution pathway are as large as 1.68, 1.91, and 1.62 eV, respectively, using the experimentally resolved stable cluster species $Au_{92}(SR)_{44}$, $Au_{12}(SR)_{12}$, $Au_{18}(SR)_{14}$, and $Au_{24}(SR)_{16}$ as the references.[38,57−59] Such large positive formation energies showed that the intermediate cluster $Au_{52}(SR)_{28}$, the $Au_{55}(SR)_{29}$ cluster, and the product $Au_{58}(SR)_{30}$-iso2 cluster were energetically less stable.

$$1/2[Au_{92}(SR)_{44} + Au_{12}(SR)_{12}] \rightarrow Au_{52}(SR)_{28} \quad (10)$$

$$1/2[Au_{92}(SR)_{44} + Au_{18}(SR)_{14}] \rightarrow Au_{55}(SR)_{29} \quad (11)$$

$$1/2[Au_{92}(SR)_{44} + Au_{24}(SR)_{16}] \rightarrow Au_{58}(SR)_{30} - iso2 \quad (12)$$

In order to further explore the possibility of cluster size-growth from Au_{49} to Au_{58}, we plotted the energy profile of this process. It is seen from Figure 7 that such a growth process needs to cross relatively high energy barriers. In light of high energy barriers during this cluster size growth pathway and the relatively low stability of the intermediate clusters, the formation of $Au_{58}(SR)_{30}$ is not supported. Although the $Au_{58}(SR)_{30}$ cluster followed the principle of symmetric growth from $Au_{40}(SR)_{24}$ to $Au_{49}(SR)_{27}$-exp, the tension between the ligand shell and the gold atom in the metal core increases significantly during the cluster size evolution, and the stability of the intermediate clusters is poor, which indicates that the formation of the $Au_{58}(SR)_{30}$ cluster is not favorable.

4. CONCLUSIONS

In conclusion, based on the $2e^-$-reduction cluster growth mechanism, the formation mechanism of the dual-packed kernel structure in the $Au_{49}(SR)_{27}$ and the $Au_{58}(SR)_{30}$ clusters was studied. The DFT energy calculation results showed that the favorable formation of dual-packed kernels in the $Au_{49}(SR)_{27}$ cluster is due to the stability of the intermediate cluster structures as well as the relatively high thermodynamic stability of the cluster itself. However, although the structure of $Au_{58}(SR)_{30}$ clusters conforms to the principle of symmetric growth, the tension between the ligand shell and the metal core gold atoms increases significantly during the cluster size evolution, and the stability of the intermediate clusters is poor, which hinders the formation of the $Au_{58}(SR)_{30}$ cluster. This study shows that it is necessary to consider the structural

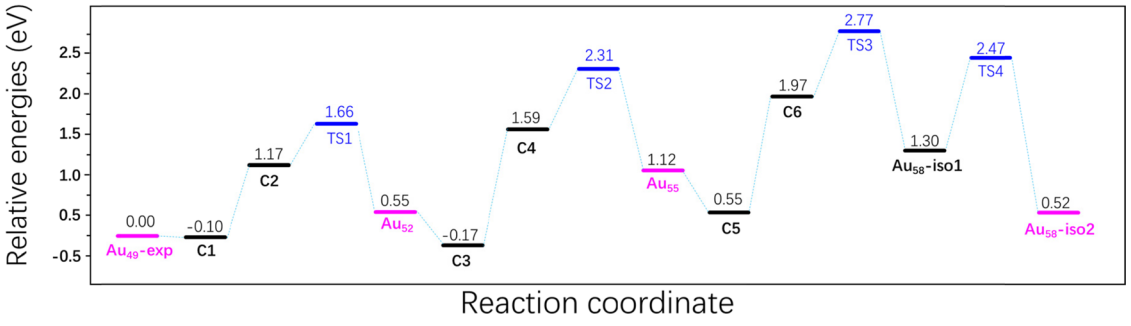

Figure 7. Energy curve of the hypothetical reaction path from Au_{49}-exp to Au_{58}-iso2. C1, C3, and C5 are cluster species formed by $Au_{49}(SR)_{27}$-exp, $Au_{52}(SR)_{28}$, and $Au_{55}(SR)_{29}$ inserted by one $[Au_3(SR)_3COOH]^-$ fragment, respectively. C2, C4, and C6 are the products of decarboxylation of $[Au_{49}(SR)_{27}$-$Au_3(SR)_3COOH]^-$, $[Au_{52}(SR)_{28}$-$Au_3(SR)_3COOH]^-$, and $[Au_{55}(SR)_{29}$-$Au_3(SR)_3COOH]^-$, respectively. TS1, TS2, and TS3 represent the TSs of motif Au collapse and nucleation. TS4 means the TS of the isomerization process from Au_{58}-iso1 to Au_{58}-iso2.

https://doi.org/10.1021/acsomega.1c01791
ACS Omega 2021, 6, 18024−18032

stability and thermodynamics of cluster formation when studying the evolution of clusters according to the symmetry growth principle. The $2e^-$reduction-assisted cluster size growth mechanism provides a good scheme for exploring the evolution path of cluster structures and evaluating the stability of clusters.

■ ASSOCIATED CONTENT

Supporting Information

The Supporting Information is available free of charge at https://pubs.acs.org/doi/10.1021/acsomega.1c01791.

Details of $Au_{46}(SR)_{26}$ and $Au_{49}(SR)_{27}$-iso cluster size-growth steps, structural isomerization of Au_{49} and Au_{58} clusters, and atomic coordinates of $Au_{43}(SCH_3)_{25}$, $Au_{46}(SCH_3)_{26}$, and $Au_{49}(SCH_3)_{27}$-iso clusters (PDF).

■ AUTHOR INFORMATION

Corresponding Author

Yong Pei − *Department of Chemistry, Key Laboratory of Environmentally Friendly Chemistry and Applications of Ministry of Education, Key Laboratory for Green Organic Synthesis and Application of Hunan Province, Xiangtan University, Xiangtan, Hunan Province 411105, China;* orcid.org/0000-0003-0585-2045; Email: ypei2@xtu.edu.cn

Author

Lin Xiong − *Department of Chemistry, Key Laboratory of Environmentally Friendly Chemistry and Applications of Ministry of Education, Key Laboratory for Green Organic Synthesis and Application of Hunan Province, Xiangtan University, Xiangtan, Hunan Province 411105, China*

Complete contact information is available at: https://pubs.acs.org/10.1021/acsomega.1c01791

Notes

The authors declare no competing financial interest.

■ ACKNOWLEDGMENTS

The authors acknowledge the financial support by NSFC (91961121, 21773201, and 21422305) and the project of innovation team of the ministry of education (IRT_17R90).

■ REFERENCES

(1) Aikens, C. M. Electronic Structure of Ligand-Passivated Gold and Silver Nanoclusters. *J. Phys. Chem. Lett.* **2011**, *2*, 99−104.

(2) Yau, S. H.; Varnavski, O.; Goodson, T., III An Ultrafast Look at Au Nanoclusters. *Acc. Chem. Res.* **2013**, *46*, 1506−1516.

(3) Jin, R.; Zeng, C.; Zhou, M.; Chen, Y. Atomically Precise Colloidal Metal Nanoclusters and Nanoparticles: Fundamentals and Opportunities. *Chem. Rev.* **2016**, *116*, 10346−10413.

(4) Kang, X.; Zhu, M. Tailoring the Photoluminescence of Atomically Precise Nanoclusters. *Chem. Soc. Rev.* **2019**, *48*, 2422−2457.

(5) Higaki, T.; Li, Y.; Zhao, S.; Li, Q.; Li, S.; Du, X. S.; Yang, S.; Chai, J.; Jin, R. Atomically Tailored Gold Nanoclusters for Catalytic Application. *Angew. Chem.* **2019**, *131*, 8377−8388.

(6) Zhou, M.; Higaki, T.; Li, Y.; Zeng, C.; Li, Q.; Sfeir, M. Y.; Jin, R. Three-Stage Evolution from Nonscalable to Scalable Optical Properties of Thiolate-Protected Gold Nanoclusters. *J. Am. Chem. Soc.* **2019**, *141*, 19754−19764.

(7) Pei, Y.; Zeng, X. C. Investigating the Structural Evolution of Thiolate Protected Gold Clusters from First-Principles. *Nanoscale* **2012**, *4*, 4054−4072.

(8) Jin, R. Atomically Precise Metal Nanoclusters: Stable Sizes and Optical Properties. *Nanoscale* **2015**, *7*, 1549−1565.

(9) Sakthivel, N. A.; Dass, A. Aromatic Thiolate-Protected Series of Gold Nanomolecules and a Contrary Structural Trend in Size Evolution. *Acc. Chem. Res.* **2018**, *51*, 1774−1783.

(10) Yao, Q.; Chen, T.; Yuan, X.; Xie, J. Toward Total Synthesis of Thiolate-Protected Metal Nanoclusters. *Acc. Chem. Res.* **2018**, *51*, 1338−1348.

(11) Xiong, L.; Yang, S.; Sun, X.; Chai, J.; Rao, B.; Yi, L.; Zhu, M.; Pei, Y. Structure and Electronic Structure Evolution of Thiolate-Protected Gold Nanoclusters Containing Quasi Face-Centered-Cubic Kernels. *J. Phys. Chem. C* **2018**, *122*, 14898−14907.

(12) Wang, P.; Xiong, L.; Sun, X.; Ma, Z.; Pei, Y. Exploring the Structure Evolution and Core/Ligand Structure Patterns of a Series of Large Sized Thiolate-Protected Gold Clusters $Au_{145-3N}(SR)_{60-2N}$ (N= 1−8): A First Principles Study. *Nanoscale* **2018**, *10*, 3918−3929.

(13) Yan, N.; Xia, N.; Liao, L.; Zhu, M.; Jin, F.; Jin, R.; Wu, Z. Unraveling the Long-Pursued Au_{144} Structure by X-ray Crystallography. *Sci. Adv.* **2018**, *4*, No. eaat7259.

(14) Nasaruddin, R. R.; Chen, T.; Yan, N.; Xie, J. Roles of Thiolate Ligands in the Synthesis, Properties and Catalytic Application of Gold Nanoclusters. *Coord. Chem. Rev.* **2018**, *368*, 60−79.

(15) Malola, S.; Häkkinen, H. Chiral Inversion of Thiolate-Protected Gold Nanoclusters via Core Reconstruction without Breaking a Au−S Bond. *J. Am. Chem. Soc.* **2019**, *141*, 6006−6012.

(16) Chevrier, D. M.; Raich, L.; Rovira, C.; Das, A.; Luo, Z.; Yao, Q.; Chatt, A.; Xie, J.; Jin, R.; Akola, J.; Zhang, P. Molecular-Scale Ligand Effects in Small Gold-Thiolate Nanoclusters. *J. Am. Chem. Soc.* **2018**, *140*, 15430−15436.

(17) Pei, Y.; Wang, P.; Ma, Z.; Xiong, L. Growth-Rule-Guided Structural Exploration of Thiolate-Protected Gold Nanoclusters. *Acc. Chem. Res.* **2019**, *52*, 23−33.

(18) Jadzinsky, P. D.; Calero, G.; Ackerson, C. J.; Bushnell, D. A.; Kornberg, R. D. Structure of a Thiol Monolayer-Protected Gold Nanoparticle at 1.1 Å Resolution. *Science* **2007**, *318*, 430−433.

(19) Kawawaki, T.; Negishi, Y.; Kawasaki, H. Photo/Electrocatalysis and Photosensitization Using Metal Nanoclusters for Green Energy and Medical Applications. *Nanoscale Adv.* **2020**, *2*, 17−36.

(20) Dou, X.; Chen, X.; Zhu, H.; Liu, Y.; Chen, D.; Yuan, X.; Yao, Q.; Xie, J. Water-Soluble Metal Nanoclusters: Recent Advances in Molecular-Level Exploration and Biomedical Applications. *Dalton Trans.* **2019**, *48*, 10385−10392.

(21) Tao, Y.; Li, M.; Ren, J.; Qu, X. Metal Nanoclusters: Novel Probes for Diagnostic and Therapeutic Applications. *Chem. Soc. Rev.* **2015**, *44*, 8636−8663.

(22) Heaven, M. W.; Dass, A.; White, P. S.; Holt, K. M.; Murray, R. W. Crystal Structure of the Gold Nanoparticle $[N(C_8H_{17})_4][Au_{25}(SCH_2CH_2Ph)_{18}]$. *J. Am. Chem. Soc.* **2008**, *130*, 3754−3755.

(23) Zhu, M.; Aikens, C. M.; Hollander, F. J.; Schatz, G. C.; Jin, R. Correlating the Crystal Structure of A Thiol-Protected Au_{25} Cluster and Optical Properties. *J. Am. Chem. Soc.* **2008**, *130*, 5883−5885.

(24) Briant, C. E.; Theobald, B. R. C.; White, J. W.; Bell, L. K.; Mingos, D. M. P.; Welch, A. J. Synthesis and X-ray Structural Characterization of the Centred Icosahedral Gold Cluster Compound $[AuI_3(PMe_2Ph)_{10}Cl_2](PF_6)_3$; the Realization of a Theoretical Prediction. *J. Chem. Soc., Chem. Commun.* **1981**, 201−202.

(25) Shichibu, Y.; Negishi, Y.; Watanabe, T.; Chaki, N. K.; Kawaguchi, H.; Tsukuda, T. Biicosahedral Gold Clusters $[Au_{25}(PPh_3)_{10}(SC_nH_{2n+1})_5Cl_2]^{2+}$ (n = 2−18): A Stepping Stone to Cluster-Assembled Materials. *J. Phys. Chem. C* **2007**, *111*, 7845−7847.

(26) Qian, H.; Eckenhoff, W. T.; Zhu, Y.; Pintauer, T.; Jin, R. Total Structure Determination of Thiolate-Protected Au_{38} Nanoparticles. *J. Am. Chem. Soc.* **2010**, *132*, 8280−8281.

(27) Qian, H.; Eckenhoff, W. T.; Bier, M. E.; Pintauer, T.; Jin, R. Crystal Structures of Au_2 Complex and Au_{25} Nanocluster and Mechanistic Insight into the Conversion of Polydisperse Nanoparticles into Monodisperse Au_{25} Nanoclusters. *Inorg. Chem.* **2011**, *50*, 10735−10739.

(28) Xu, W. W.; Zhu, B.; Zeng, X. C.; Gao, Y. A Grand Unified Model for Liganded Gold Clusters. *Nat. Commun.* **2016**, *7*, 13574.
(29) Chen, S.; Xiong, L.; Wang, S.; Ma, Z.; Jin, S.; Sheng, H.; Pei, Y.; Zhu, M. Total structure determination of $Au_{21}(S\text{-}Adm)_{15}$ and geometrical/electronic structure evolution of thiolated gold nanoclusters. *J. Am. Chem. Soc.* **2016**, *138*, 10754−10757.
(30) Das, A.; Li, T.; Nobusada, K.; Zeng, C.; Rosi, N. L.; Jin, R. Nonsuperatomic $[Au_{23}(SC_6H_{11})_{16}]^-$ Nanocluster Featuring Bipyramidal Au_{15} Kernel and Trimeric $Au_3(SR)_4$ Motif. *J. Am. Chem. Soc.* **2013**, *135*, 18264−18267.
(31) Zeng, C.; Liu, C.; Chen, Y.; Rosi, N. L.; Jin, R. Gold−thiolate ring as a protecting motif in the $Au_{20}(SR)_{16}$ nanocluster and implications. *J. Am. Chem. Soc.* **2014**, *136*, 11922−11925.
(32) Chen, Y.; Liu, C.; Tang, Q.; Zeng, C.; Higaki, T.; Das, A.; Jiang, D.; Rosi, N. L.; Jin, R. Isomerism in $Au_{28}(SR)_{20}$ Nanocluster and Stable Structures. *J. Am. Chem. Soc.* **2016**, *138*, 1482−1485.
(33) Xiong, L.; Peng, B.; Ma, Z.; Wang, P.; Pei, Y. A Ten-Electron (10e) Thiolate-Protected $Au_{29}(SR)_{19}$ cluster: Structure Prediction and a 'Gold-Atom Insertion, Thiolate-Group Elimination' Mechanism. *Nanoscale* **2017**, *9*, 2895−2902.
(34) Li, Y.; Zhou, M.; Song, Y.; Higaki, T.; Wang, H.; Jin, R. Double-helical assembly of heterodimeric nanoclusters into supercrystals. *Nature* **2021**, *594*, 380−384.
(35) Dass, A.; Jones, T.; Rambukwella, M.; Crasto, D.; Gagnon, K. J.; Sementa, L.; De Vetta, M.; Baseggio, O.; Aprà, E.; Stener, M.; Fortunelli, A. Crystal Structure and Theoretical Analysis of Green Gold $Au_{30}(S\text{-}tBu)_{18}$ Nanomolecules and Their Relation to $Au_{30}S(S\text{-}tBu)_{18}$. *J. Phys. Chem. C* **2016**, *120*, 6256−6261.
(36) Zeng, C.; Chen, Y.; Iida, K.; Nobusada, K.; Kirschbaum, K.; Lambright, K. J.; Jin, R. Gold Quantum Boxes: On the Periodicities and the Quantum Confinement in the Au_{28}, Au_{36}, Au_{44}, and Au_{52} Magic Series. *J. Am. Chem. Soc.* **2016**, *138*, 3950−3953.
(37) Wang, P.; Sun, X.; Liu, X.; Xiong, L.; Ma, Z.; Pei, Y. Theoretical Predictions of a New ∼14 kDa Core-Mass Thiolate-Protected Gold Nanoparticle: $Au_{68}(SR)_{36}$. *J. Phys. Chem. Lett.* **2017**, *8*, 1248−1252.
(38) Zeng, C.; Liu, C.; Chen, Y.; Rosi, N. L.; Jin, R. Atomic Structure of Self-Assembled Monolayer of Thiolates on a Tetragonal Au_{92} Nanocrystal. *J. Am. Chem. Soc.* **2016**, *138*, 8710−8713.
(39) Liao, L.; Zhuang, S.; Yao, C.; Yan, N.; Chen, J.; Wang, C.; Xia, N.; Liu, X.; Li, M.-B.; Li, L.; Bao, X.; Wu, Z. Structure of Chiral $Au_{44}(2,4\text{-}DMBT)_{26}$ Nanocluster with an 18-Electron Shell Closure. *J. Am. Chem. Soc.* **2016**, *138*, 10425−10428.
(40) Liao, L.; Zhuang, S.; Wang, P.; Xu, Y.; Yan, N.; Dong, H.; Wang, C.; Zhao, Y.; Xia, N.; Li, J.; Deng, H.; Pei, Y.; Tian, S.-K.; Wu, Z. Quasi-Dual-Packed-Kerneled $Au_{49}(2,4\text{-}DMBT)_{27}$ Nanoclusters and the Influence of Kernel Packing on the Electrochemical Gap. *Angew. Chem., Int. Ed.* **2017**, *56*, 12644−12648.
(41) Tian, S.; Li, Y.-Z.; Li, M.-B.; Yuan, J.; Yang, J.; Wu, Z.; Jin, R. Structural Isomerism in Gold Nanoparticles Revealed by X-ray Crystallography. *Nat. Commun.* **2015**, *6*, 8667.
(42) Zeng, C.; Chen, Y.; Liu, C.; Nobusada, K.; Rosi, N. L.; Jin, R. Gold Tetrahedra Coil Up: Kekulé-like and Double Helical Superstructures. *Sci. Adv.* **2015**, *1*, No. e1500425.
(43) Xu, W.-W.; Zheng, M. Medium-Sized $Au_{58}(SR)_{30}$: A New Chiral Structure Evolving from Crystallized $Au_{40}(SR)_{24}$ and $Au_{49}(SR)_{27}$. *J. Phys. Chem. C* **2020**, *124*, 9077−9081.
(44) Peng, J.; Wang, P.; Wang, B.; Xiong, L.; Liu, H.; Pei, Y.; Zeng, X. C. Exploration of Formation and Size-Evolution Pathways of Thiolate-Gold Nanoclusters in the CO-Directed $[Au_{25}(SR)_{18}]^-$ Synthesis. *Small* **2020**, No. 2000627.
(45) Perdew, J. P.; Burke, K.; Ernzerhof, M. Generalized Gradient Approximation Made Simple. *Phys. Rev. Lett.* **1996**, *77*, 3865−3868.
(46) Delley, B. An All-Electron Numerical Method for Solving the Local Density Functional for Polyatomic Molecules. *J. Chem. Phys.* **1990**, *92*, 508−517.
(47) Delley, B. From Molecules to Solids with the $DMol^3$ Approach. *J. Chem. Phys.* **2000**, *113*, 7756−7764.
(48) Tkatchenko, A.; Scheffler, M. Accurate Molecular Van Der Waals Interactions from Ground-State Electron Density and Free-Atom Reference Data. *Phys. Rev. Lett.* **2009**, *102*, No. 073005.
(49) Dolney, D. M.; Hawkins, G. D.; Winget, P.; Liotard, D. A.; Cramer, C. J.; Truhlar, D. G. Universal Solvation Model Based on Conductor-Like Screening Model. *J. Comput. Chem.* **2000**, *21*, 340−366.
(50) *ADF2010.01, SCM, Theoretical Chemistry*; Vrije Universiteit: Amsterdam, The Netherlands. http://www.scm.com.
(51) Pei, Y.; Gao, Y.; Zeng, X. C. Structural Prediction of Thiolate-Protected Au_{38}: A Face-Fused Bi-icosahedral Au Core. *J. Am. Chem. Soc.* **2008**, *130*, 7830−7832.
(52) Häkkinen, H.; Walter, M.; Grönbeck, H. Divide and Protect: Capping Gold Nanoclusters with Molecular Gold−Thiolate Rings. *J. Phys. Chem. B* **2006**, *110*, 9927−9931.
(53) Yao, Q.; Yuan, X.; Fung, V.; Yu, Y.; Leong, D. T.; Jiang, D.; Xie, J. Understanding Seed-Mediated Growth of Gold Nanoclusters at Molecular Level. *Nat. Commun.* **2017**, *8*, 927.
(54) Dong, H.; Liao, L.; Wu, Z. Two-Way Transformation between fcc- and Nonfcc-Structured Gold Nanoclusters. *J. Phys. Chem. Lett.* **2017**, *8*, 5338−5343.
(55) Luo, Z.; Nachammai, V.; Zhang, B.; Yan, N.; Leong, D. T.; Jiang, D.; Xie, J. Toward Understanding the Growth Mechanism: Tracing All Stable Intermediate Species from Reduction of Au(I)−Thiolate Complexes to Evolution of Au_{25} Nanoclusters. *J. Am. Chem. Soc.* **2014**, *136*, 10577−10580.
(56) Eyring, H. The Activated Complex in Chemical Reactions. *J. Chem. Phys.* **1935**, *3*, 107−115.
(57) Das, A.; Liu, C.; Byun, H. Y.; Nobusada, K.; Zhao, S.; Rosi, N.; Jin, R. Structure Determination of $[Au_{18}(SR)_{14}]$. *Angew. Chem., Int. Ed.* **2015**, *54*, 3140−3144.
(58) Crasto, D.; Barcaro, G.; Stener, M.; Sementa, L.; Fortunelli, A.; Dass, A. $Au_{24}(SAdm)_{16}$ Nanomolecules: X-ray Crystal Structure, Theoretical Analysis, Adaptability of Adamantane Ligands to Form $Au_{23}(SAdm)_{16}$ and $Au_{25}(SAdm)_{16}$, and Its Relation to $Au_{25}(SR)_{18}$. *J. Am. Chem. Soc.* **2014**, *136*, 14933−14940.
(59) Xu, G. T.; Wu, L. L.; Chang, X. Y.; Ang, T. W. H.; Wong, W. Y.; Huang, J. S.; Che, C. M. Solvent-Induced Cluster-to-Cluster Transformation of Homoleptic Gold(I) Thiolates between Catenane and Ring-in-Ring Structures. *Angew. Chem., Int. Ed.* **2019**, *131*, 16443−16452.

https://doi.org/10.1021/acsomega.1c01791
ACS Omega 2021, 6, 18024−18032